



Surround suppression supports second-order feature encoding by macaque V1 and V2 neurons



Luke E. Hallum*, J. Anthony Movshon

Center for Neural Science, New York University, New York, NY 10003, United States

ARTICLE INFO

Article history:

Received 22 July 2014

Received in revised form 30 September 2014

Available online 23 October 2014

Keywords:

Surround suppression

Second-order

Primary visual cortex

V2

Receptive field

Filter-rectify-filter

ABSTRACT

Single neurons in areas V1 and V2 of macaque visual cortex respond selectively to luminance-modulated stimuli. These responses are often influenced by context, for example when stimuli extend outside the classical receptive field (CRF). These contextual phenomena, observed in many sensory areas, reflect a fundamental cortical computation and may inform perception by signaling second-order visual features which are defined by spatial relationships of contrast, orientation and spatial frequency. In the anesthetized, paralyzed macaque, we measured single-unit responses to a drifting preferred sinusoidal grating; low spatial frequency sinusoidal contrast modulations were applied to the grating, creating contrast-modulated, second-order forms. Most neurons responded selectively to the orientation of the contrast modulation of the preferred grating and were therefore second-order orientation-selective. Second-order selectivity was created by the asymmetric spatial organization of the excitatory CRF and suppressive extraclassical surround. We modeled these receptive field subregions using spatial Gaussians, sensitive to the modulation of contrast (not luminance) of the preferred carrier grating, that summed linearly and were capable of recovering asymmetrical receptive field organizations. Our modeling suggests that second-order selectivity arises both from elongated excitatory CRFs, asymmetrically organized extraclassical surround suppression, or both. We validated the model by successfully testing its predictions against conventional surround suppression measurements and spike-triggered analysis of second-order form responses. Psychophysical adaptation measurements on human observers revealed a pattern of second-order form selectivity consistent with neural response patterns. We therefore propose that cortical cells in primates do double duty, providing signals about both first- and second-order forms.

© 2014 Elsevier Ltd. All rights reserved.

1. Introduction

The classical receptive fields (CRFs) of neurons in monkey visual cortex (areas V1 and V2) are selectively sensitive to the orientation and spatial frequency of a sinusoidal grating (De Valois, William Yund, & Hepler, 1982; Levitt, Kiper, & Movshon, 1994). Neuronal responses are also often modulated by the visual context in which they appear. A simple example is surround suppression: if a grating presented to the CRF extends into the surrounding extraclassical receptive field, the response is reduced (Cavanaugh, Bair, & Movshon, 2002a, 2002b; Henry et al., 2013; Kim & Freeman, 2014; Sceniak et al., 1999; Shushruth et al., 2013). Contextual responses are found in many sensory cortical areas, and are likely to represent a fundamental computation for a range of perceptual and motor behaviors (Carandini & Heeger, 2013). Here, we

examine the temporal and spatial properties of the neural mechanisms implementing these contextual responses in primate cortex, with a particular focus on whether contextual mechanisms can confer sensitivity to “second-order” visual features.

Human observers are sensitive to first-order features defined by changes in luminance, for example, a border between light and dark. But we are also sensitive to features defined by differences between first-order cues, for example, a “herringbone” border between perpendicular textures, or a border between textures of the same orientation but differing spatial frequency content (reviewed by Graham, 2011; Graham & Sutter, 1998; Landy & Graham, 2004). This second-order sensitivity plays a fundamental role in vision, because spatial and temporal information can be conveyed by many image properties – among them luminance, color, contrast, disparity, and texture – which in isolation or in combination (Saarela & Landy, 2012) affect an observer’s ability to locate and identify objects. This ability can be explained by a “filter-rectify-filter” (FRF) model (Ellemberg, Allen, & Hess, 2006; Graham & Sutter, 1998; Graham & Wolfson, 2004; Landy &

* Corresponding author at: Center for Neural Science, New York University, 4 Washington Place, Room 809, New York, NY 10003, United States.

E-mail address: hallum@cns.nyu.edu (L.E. Hallum).

Bergen, 1991; Landy & Oruç, 2002; Langley, Fleet, & Hibbard, 1996; McGraw, Levi, & Whitaker, 1999; Schofield & Georgeson, 1999). This model postulates two cascaded stages. The first is a linear spatiotemporal filter which gives an orientation- and spatial frequency-selective response to luminance. The rectified output of this filter is passed to a second linear filter which responds selectively to variations in the outputs of the first-order filters and represents this variation across regions of an image.

How could contextual mechanisms confer sensitivity to second-order features? Contextual responses represent a complex sensory transformation which modifies the basic orientation and spatial frequency selectivity of neurons. These contextual modulations may play an important role in the perception of complex spatial forms. In particular, when a neuron's RF is organized asymmetrically (Cavanaugh, Bair, & Movshon, 2002a, 2002b; Tanaka & Ohzawa, 2009; Walker, Ohzawa, & Freeman, 1999) its responses can signal the form of second-order visual features. We wondered to what extent the RF was organized anisotropically in macaque V1 and V2 neurons, and whether the FRF model might account for the activity of single units, so we used the method of Tanaka and Ohzawa (2009) to probe the receptive fields of neurons in macaque V1 and V2. Our results suggest that as in cat (Tanaka & Ohzawa, 2009), contextual modulation may account for some forms of second-order sensitivity in primate cortex.

2. Methods

2.1. Subjects and surgical preparation

We recorded from 10 macaques (*Macaca nemestrina* and *Macaca fascicularis*; 1 female and 9 males). Animals were prepared for recording as described previously (Cavanaugh, Bair, & Movshon, 2002a). Experiments typically lasted 5 days, during which anesthesia and paralysis were maintained with continuous intravenous infusion of sufentanil citrate (initially 6 $\mu\text{g}/\text{kg}/\text{h}$, adjusted thereafter to maintain a suitable level of anesthesia for each animal) and vecuronium bromide (Norcuron; 0.1 $\text{mg}/\text{kg}/\text{h}$) in isotonic dextrose-Normosol solution. Vital signs were constantly monitored (electroencephalograph, blood pressure, heart rate, lung pressure, end-tidal pCO_2 , temperature, and urine flow and osmolarity) and actively maintained within appropriate physiological limits. Pupils were dilated with topical atropine and the eyes were protected with oxygen-permeable contact lenses. Supplementary lenses chosen via direct ophthalmoscopy were used to make the retinas conjugate with the experimental display. All animal care and experimental procedures were performed in accordance with protocols approved by the New York University Animal Welfare Committee and conformed to the National Institute of Health *Guide for the Care and Use of Laboratory Animals*.

2.2. Unit recording

We made extracellular recordings with quartz-coated, platinum-tungsten microelectrodes (Thomas Recording) advanced mechanically through a craniotomy and durotomy centered 2–4 mm posterior to the lunate sulcus and 10–16 mm lateral to the midline. Electrode penetrations were confined to a parasagittal plane and directed downward at an angle of 20 deg from vertical. We identified area V2 by (1) marking gray matter as we traversed surface cortex, followed by a stretch of white matter before reaching V2 on the posterior bank of the lunate sulcus; (2) tracking changes in visual topography along the recording track: receptive fields in surface V1 were located close to the vertical meridian; V2 receptive fields were at 2–5° of visual eccentricity; (3) marking cortical depth along the recording track: at our typical sites, V2

was found 2500–3500 μm from brain surface. Signals from the microelectrodes were amplified, bandpass-filtered (300 Hz to 10 kHz), and fed into a dual window time–amplitude discriminator for spike detection. Spike times were saved with a temporal resolution of 0.1 ms.

2.3. Visual stimulation

We presented stimuli on a gamma-corrected cathode ray tube (CRT) monitor (Eizo T966), with spatial resolution 1280 \times 960 pixels, temporal resolution 120 Hz, and mean luminance 35 cd/m^2 . Viewing distance was usually 1.14 m. Stimuli were generated using an Apple Macintosh running Expo (<http://corevision.cns.nyu.edu>).

For each neuron, we hand-mapped the receptive field of each eye on a tangent screen. After qualitatively determining ocular dominance, we presented stimuli monocularly to the dominant eye, occluding its fellow. We first determined selectivity for direction, spatial frequency, and temporal frequency of a small, circular patch of high-contrast sinusoidal grating presented to the putative classical receptive field (CRF). Using these parameters, we measured responses to second-order stimuli.

We created second-order stimuli by multiplying a sinusoidal “carrier” grating by a raised, sinusoidal “modulator” grating (Fig. 1). The “preferred” carrier grating took the spatial frequency and drift direction determined found to be optimal during initial mapping. We usually set the temporal frequency of the carrier to

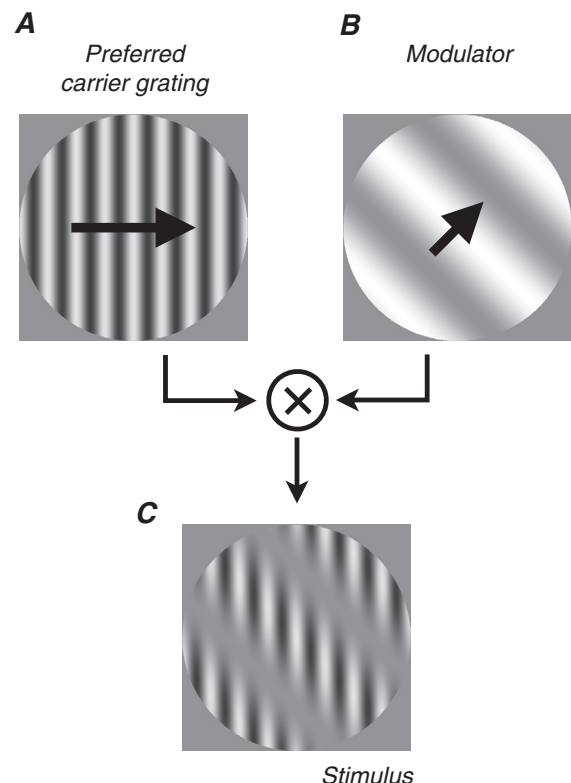


Fig. 1. Stimulus construction. We modulated the contrast of a large, circular patch of sinusoidal carrier grating (A) using a relatively low spatial frequency, raised sinusoidal modulator (B) forming the second-order stimulus (C). We optimized the carrier grating's orientation and spatial frequency for each neuron, and typically set its drift rate to approximately 5 Hz. The modulator always drifted at 0.75 Hz. The contrasts of the carrier grating and the modulator were 75% and 100%, respectively. In each experiment, from trial to trial, we varied the modulator's drift direction (0, 45, 90, ... 315 deg relative to the carrier grating's drift direction) and the modulator's spatial frequency (0, 0.125, 0.25, ... 0.75 \times the carrier grating's spatial frequency). Shown here the modulator drifts at 45 deg relative to the carrier with spatial frequency 0.25 \times .

approximately 5 Hz which usually elicited vigorous firing. Occasionally we used a higher drift rate if that proved more effective. We used contrast modulations of the preferred carrier grating only, and set its peak contrast to 0.75. The parameters governing the preferred carrier grating were fixed while the spatial frequency and drift direction of the modulator were systematically varied across trials. Stimuli appeared within a circular window with softened edges and a diameter equal to eight carrier cycles, approximately centered on the neuron's CRF. We used modulator spatial frequencies at 0, 0.125, 0.25, ... $0.75 \times$ the preferred carrier grating's spatial frequency, and modulator drift directions 0, 45, 90, ... 315 deg relative to the preferred carrier grating's drift direction. The drift rate of the modulator was always 0.75 Hz. Trials were 4 s in duration, and followed one another without interruption. The spatial frequencies and drift directions of the modulators were randomly interleaved from trial to trial.

For many neurons, a second validation experiment was interleaved with the main experiment to make conventional measurements of areal summation (Cavanaugh, Bair, & Movshon, 2002a; Sceniak et al., 1999). The preferred grating was presented in a circular window with softened edges and a diameter which was varied over trials, taking values 0, 0.17, 0.33, ... 1.0 times the stimulus diameter that was used in the main experiment. The overall contrast of the circular stimulus was modulated at 0.75 Hz.

2.4. Analysis

2.4.1. Response estimates and response variability

We estimated the fundamental (0.75 Hz) component of neuronal responses to the modulator (Fig. 1). We pooled all trials of a particular type (e.g., modulator spatial frequency equal to 0.25 times the preferred carrier grating's spatial frequency and modulator drift direction equal to 60 deg) and, with each spike, formed a unit-length vector in the complex plane with azimuth proportional to the spatial phase of the modulator at the time of the spike's occurrence. The vector sum was used to compute the fundamental response (0.75 Hz). We estimated the variance of that estimate by bootstrapping. For each trial type, we sampled with replacement the spike times of each trial. We then re-computed the fundamental response component. This procedure was repeated 2000 times providing an empirical distribution of the fundamental response. To estimate the standard error of the fundamental response, we computed the standard deviation of the amplitudes of the vectors comprising this distribution.

2.4.2. Latency estimates

We estimated the response latency of a neuron to contrast modulations of the preferred carrier grating as follows. Responses were often selective for the modulator's orientation, but not its direction. So we assumed a neuron's temporal response to a drifting modulator, and its response to the otherwise identical modulator drifting in the opposite direction, were time-reversed copies of each other. That is, after accounting for response latency, these two fundamental responses form a conjugate pair in the complex plane and sum to give a complex number with an imaginary component of zero. For each neuron, first, we assumed a latency of 0 ms, computing the fundamental responses on every trial of the experiment. We summed these fundamental responses, and computed the imaginary component of that sum. We repeated this procedure for assumed latencies of ranging between 0 ms and 200 ms. We plotted the imaginary component versus latency and fitted a sinusoid with temporal frequency 0.75 Hz. The zero crossing of this fitted sinusoid provided the response latency estimate.

2.4.3. Orientation- and direction-selectivity index

We quantified each neuron's response selectivity for modulator orientation using an orientation-selectivity index (OSI): $OSI = 1 - CV_{2\theta}$. Term $CV_{2\theta}$ denotes circular variance averaged over neuronal responses to stimuli that drift in opposite directions, but are otherwise identical (Ringach, Hawken, & Shapley, 1997). We computed the amplitude of the fundamental Fourier component of the response to each trial. The OSI was computed using an average of these response amplitudes within modulator drift direction at each modulator spatial frequency. We then used a Bonferroni-corrected (one test at each modulator spatial frequency) permutation test, shuffling labels on individual trials (criterion $p < 0.05$) to assess the robustness of the OSI. The direction-selectivity index (DSI) was computed for each neuron analogously to the OSI: $DSI = 1 - CV_{\theta}$. The term CV_{θ} denotes circular variance that does not average neuronal responses to stimuli drifting in opposite directions.

2.5. Model

We modeled the spatial organization of excitatory classical receptive field (CRF) centers and suppressive extraclassical surrounds using the approach devised by Tanaka and Ohzawa (2009). The model involved the difference of two spatial Gaussians (DoG), giving a center-surround field constrained by 12 parameters:

$$g(x, y) = g_c(x, y) - g_s(x, y)$$

$$g_c(x, y) = A_c \exp \left[\frac{-(x - \mu_{cx})^2}{2\sigma_{cx}^2} + \frac{-(y - \mu_{cy})^2}{2\sigma_{cy}^2} \right]$$

$$g_s(x, y) = A_s \exp \left[\frac{-(x - \mu_{sx})^2}{2\sigma_{sx}^2} + \frac{-(y - \mu_{sy})^2}{2\sigma_{sy}^2} \right]$$

The term A_c specifies the gain of the positive-going Gaussian. Terms μ_{cx} and μ_{cy} specify the position in x and y , respectively, of the positive-going Gaussian relative to the center of the stimulus. Terms σ_{cx} and σ_{cy} specify the radius of the positive-going Gaussian in the x and y directions, respectively. The five other similarly labelled terms pertain to the negative-going Gaussian. Each gaussian was allowed to rotate about its offset position; the two parameters specifying these rotations are omitted for clarity.

A DoG is commonly used to model the spatial organization and sensitivity of the retinal ganglion cell's RF to luminance variations (e.g., Enroth-Cugell & Robson, 1966; Rodieck & Stone, 1965). Here, we used a DoG in a different context: to model the spatial organization and sensitivity of cortical neurons to modulations of contrast of a preferred carrier grating. We use "preferred carrier grating" to refer to a large grating, stimulating both the neuron's CRF and suppressive surround, at a spatial frequency and drift direction eliciting the highest firing rate in preliminary hand-mapping. The DoG function performs a localized sum of changes in the contrast, Δc , of a preferred carrier grating over the center-surround RF. An example, in which two spatial Gaussians are differenced, is shown in Fig. 4B and discussed in detail in Section 3.

To find the model parameters that best accounted for measured responses (simultaneously at all modulator spatial frequencies and orientations) we evaluated the probability of the model by computing the log likelihood as follows:

$$\log L = \log \prod_i p(o_i | e_i)$$

where i indexes different modulators, e is the model's response to that modulator, o is the observed response to that modulator, and p denotes probability density function. For each neuron, multiple fits were performed using different starting parameters. Parameters

were adjusted iteratively by the Nelder-Mead optimization algorithm. We often compared the goodness-of-fit of two different models of the same neuronal responses: the full, 12-parameter model and a “no suppression”, 6-parameter model involving only one excitatory spatial Gaussian.

2.6. Psychophysics

We measured the effect of adaptation on human observers' detection and discrimination thresholds of eccentric stimuli like those used in our physiology experiment. The two psychophysical subjects (one of whom was author L.H.) had normal vision, and viewed the stimulus monocularly with the dominant eye. The observers gave informed consent to their participation in the experiments.

Stimuli (4 deg diameter centered at 5 deg eccentricity in the lower, left visual field) were contrast-modulated sinusoidal carrier gratings, as in Fig. 1. The sinusoidal carrier grating was 2 c/deg, orientation 45 deg, and contrast 0.8. The raised sinusoidal modulator was spatial frequency 0.5 c/deg, and orientation either vertical (0 deg) or horizontal (90 deg). When we used contrast-modulated stimuli as adapters, the contrast of the modulator was 1 and we independently re-randomized the spatial phases of the carrier and modulator every 0.25 s. We also used ordinary sinusoidal carrier gratings as adapters, re-randomizing spatial phase every 0.25 s. These ordinary sinusoidal carrier gratings had spatial frequency 0.5 c/deg and orientation either vertical or horizontal. First- and second-order adapters were matched for root-mean-square contrast. Adapters were presented for 60 s at the beginning of each 80-trial block, and for 4 s at the end of each trial (a so-called “top-up” interval).

Each block of two-by-two-alternative, forced-choice (2×2 AFC) trials (Watson & Robson, 1981) used one of four adapters: second-order vertical; second-order horizontal; first-order vertical; or, first-order horizontal (Fig. 8, adapter icons). Trials comprised two 150-ms stimulus intervals, each followed by a 400-ms blank interval during which we presented a uniform, mean-luminance field. During the top-up interval the subject indicated, with a first button press, which interval had contained the target, and, with a second button press, whether the target had been second-order vertical or second-order horizontal. We used two “two-down, one-up” staircases to control second-order contrast: two successive detections of a vertical (horizontal) second-order target decreased vertical (horizontal) second-order target contrast; the failure to detect a vertical (horizontal) target increased vertical (horizontal) second-order target contrast.

We estimated detection thresholds as in Wichmann and Hill (2001a, 2001b). To mitigate any effect of the adapting stimulus on response bias, we estimated discrimination thresholds using methods drawn from signal detection theory (Green & Swets, 1966; Tanner & Swets, 1954). We assumed that on each trial the subject integrated each orientation-tuned, second-order channel's activity over the two temporal intervals. We computed sensitivity by first labeling trials as “parallel” (the target's orientation was parallel to the adapter's) or “orthogonal” (the target's orientation was orthogonal to the adapter's). Then we considered a “parallel” response to a parallel target as a hit, and a “parallel” response to an orthogonal target as a false alarm, computing $d' = z(\text{hit rate}) - z(\text{false-alarm rate})$, where d' denotes sensitivity and z denotes z -score transformation. We fitted a Naka-Rushton function (e.g., Ross & Speed, 1991) and we report the second-order contrast giving $d' = 1$ as the discrimination threshold.

All the work reported in this paper was carried out in accordance with the Code of Ethics of the World Medical Association (Declaration of Helsinki).

3. Results

We recorded the responses of 61 neurons in V1 and 74 neurons in V2. We quantified the second-order orientation- and direction-selectivity of all neurons, and modeled the center-surround receptive fields of neurons that were sufficiently responsive and amenable to modeling over the range of modulator spatial frequencies that we tested. The receptive fields of all neurons encountered were between 2 and 5 deg parafoveal, responding to stimuli presented in the lower visual field.

3.1. Modulator selectivity

Neurons in V1 and V2 typically respond in an orientation-selective way to luminance modulations, e.g., a sinusoidal grating. In Fig. 2A, we show an orientation tuning curve for V1 neuron *m628r24(V1)*. We determined the approximate location and size of the neuron's CRF, and its spatial frequency and orientation preference (1.58 c/deg and 157 deg, respectively), by hand-mapping with a small, circular patch of high-contrast sinusoidal grating. Then, we recorded the responses shown in Fig. 2A which exhibit an orientation preference for a sinusoidal grating. For neuron *m628r24(V1)*, and all other neurons presented in this manuscript, we have rotated the data so that the preferred grating is vertical and drifting to the right (0 deg). We refer to the tuning curve of Fig. 2A as “first-order” since it shows responses to luminance modulations.

Many of the neurons we isolated responded selectively to “second-order” features, in addition to responding selectively to first-order features; when stimuli were large, encompassing both the excitatory CRF and the suppressive extraclassical surround, many neurons reliably signaled the orientation of a contrast modulation applied to the preferred carrier grating (e.g., Fig. 1). In Fig. 2B, we show a second-order orientation tuning curve for neuron, *m628r24(V1)*, the same neuron which furnished the first-order tuning curve of Fig. 2A. We populated this second-order tuning curve by pooling responses to identical trial types in the main experiment and computing the component at the drift rate of the second-order fundamental (0.75 Hz; see Section 2). The curve shows response amplitudes. For clarity, response phases are not shown, however they are nonetheless important in modeling the spatial and temporal organization of the center-surround RF, which we discuss below. In Fig. 2C and D, we show the first- and second-order orientation tuning curves, respectively, for V2 neuron *m628r48(V2)*.

The responses of many neurons, like the responses of neuron *m628r24(V1)*, were second-order orientation-selective. The second-order orientation selectivity index (OSI) of the responses plotted in Fig. 2B is 0.15, which passed a permutation test for selectivity ($p < 0.05$; Section 2). The second-order OSI of the responses plotted in Fig. 2D is 0.09 ($p > 0.05$). As with the responses of these two neurons, *m628r24(V1)* and *m628r48(V2)*, we computed all neurons' second-order OSI at the moderate modulator spatial frequency, i.e., $0.5 \times$ the preferred carrier grating's spatial frequency. As shown in Fig. 3A, some 36 of 60 V1 neurons (60%) and some 32 of 74 V2 neurons (43%) were second-order orientation-selective. Neurons were rarely selective for modulator direction; we computed the second-order direction-selectivity index and found only three of 135 to be statistically significant. This contrasts with earlier results from our laboratory showing a substantial number of cells with significant second-order direction selectivity (El-Shamayleh & Movshon, 2011); we assume the differences are due to differences in stimulus configuration and temporal dynamics between the two studies.

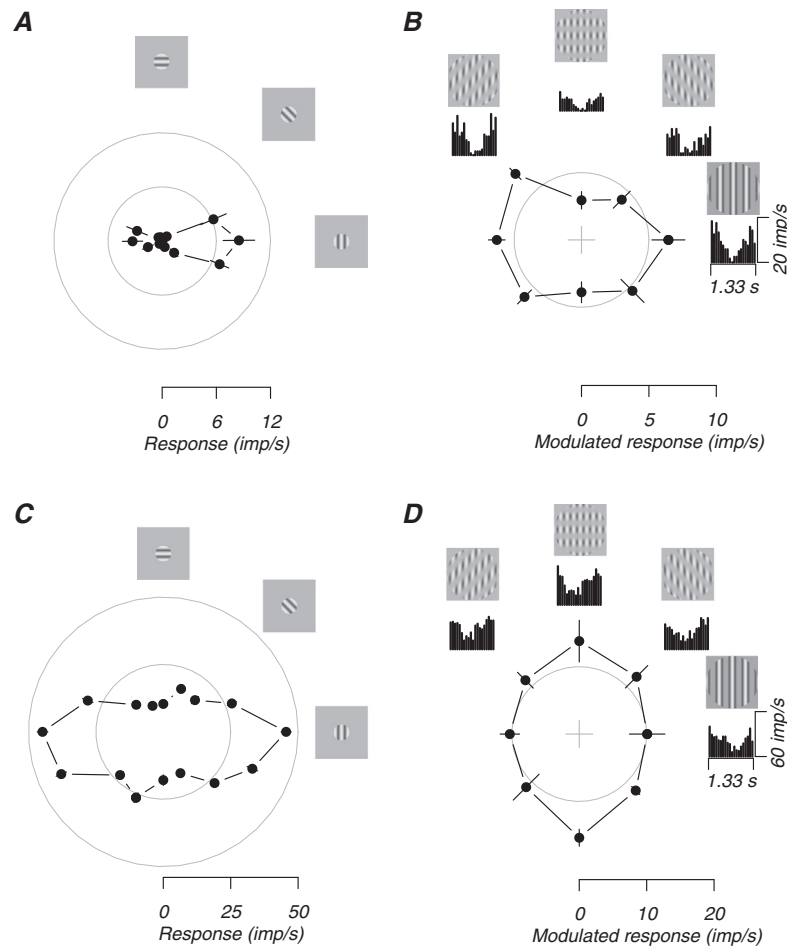


Fig. 2. First- and second-order orientation-selectivity. (A) Polar plot of “first-order” orientation-tuned responses of neuron *m628r24(V1)* to a small, circular patch of high-contrast, drifting sinusoidal grating (1.58 c/deg) presented to the classical receptive field (CRF) approximated during hand-mapping. This neuron preferred a grating drifting at 157 deg; here, and in all subsequent plots, we have rotated the data so that the preferred grating is represented as vertical and drifting to the right. (B) Polar plot of “second-order” orientation-tuned responses of the same neuron to sinusoidal contrast modulations (0.79 c/deg) of a large patch (5.1 deg) of carrier grating. For each data point, angle of elevation and radial distance indicate the modulator’s drift direction and the neuron’s modulated response amplitude, respectively. The cycle histograms beneath each stimulus icon show how the spike rate synchronized to the passage of the modulator, which drifted at temporal frequency 0.75 Hz (period = 1.33 s), over the CRF and extraclassical surround. As shown, fundamental (0.75 Hz) response amplitudes reliably signaled the orientation of the contrast modulation. Here, the second-order orientation selectivity index, OSI = 0.15 ($p < 0.05$). (C) First-order orientation-tuned responses of V2 neuron *m628r48(V2)*. The drift direction and spatial frequency of the carrier grating were 202 deg and 1.58 c/deg, respectively. (D) Second-order orientation-tuned responses of *m628r48(V2)* for modulator spatial frequency = 0.79 c/deg. Here, second-order OSI = 0.09 ($p > 0.05$). Error bars show standard error of the mean across trials.

3.2. Model

To explore the mechanisms governing second-order orientation-selectivity, we modeled the CRF and the extraclassical surround as spatially distinct excitatory and suppressive mechanisms sensitive to contrast modulations of the preferred carrier grating (Section 2). In Fig. 4A, we plot second-order spatial frequency tuning curves for a single neuron, *m628r24(V1)* (see also Fig. 2A and B). We pooled the neuron’s responses to modulators that drifted in opposite directions, but were otherwise identical; the colors pertain to different modulator orientations. We show the model fit with solid curves.

We inverse Fourier transformed the (frequency-domain) model fit, revealing the spatial organization of the center-surround RF governing responses to contrast modulations of the preferred carrier grating (Fig. 4B). The red subregion is an estimate of the shape and sensitivity of the CRF. The blue subregion estimates the extra-classical suppressive surround. We emphasize that this field should not be confused with the CRF of a classical simple cell, which has non-overlapping subregions that are sensitive to changes in luminance. The field illustrated in Fig. 4B, however,

has subregions that are sensitive to changes in contrast, not luminance – specifically, changes in contrast of the preferred carrier grating. Fig. 4C illustrates a stimulus that would elicit a vigorous response from this neuron. There, we superimposed the contours of the modeled center-surround RF on a large patch of preferred grating. We modulated that grating so that the contrast within the CRF (red) increased, thus increasing the neuronal response. In the suppressive surround, and especially at the most sensitive area of the surround, the contrast of the preferred grating was attenuated, releasing the neuron from strong surround suppression. In other words, this field was clearly selective for vertical contrast modulations of the preferred grating, which reconciles with the second-order tuning curve in Fig. 2B.

3.3. Population properties

We modeled the center-surround RFs of 58 neurons, revealing the spatial organization of the mechanisms governing surround suppression and second-order orientation-selectivity. These were the neurons that were sufficiently responsive and amenable to modeling over the range of modulator spatial frequencies tested.

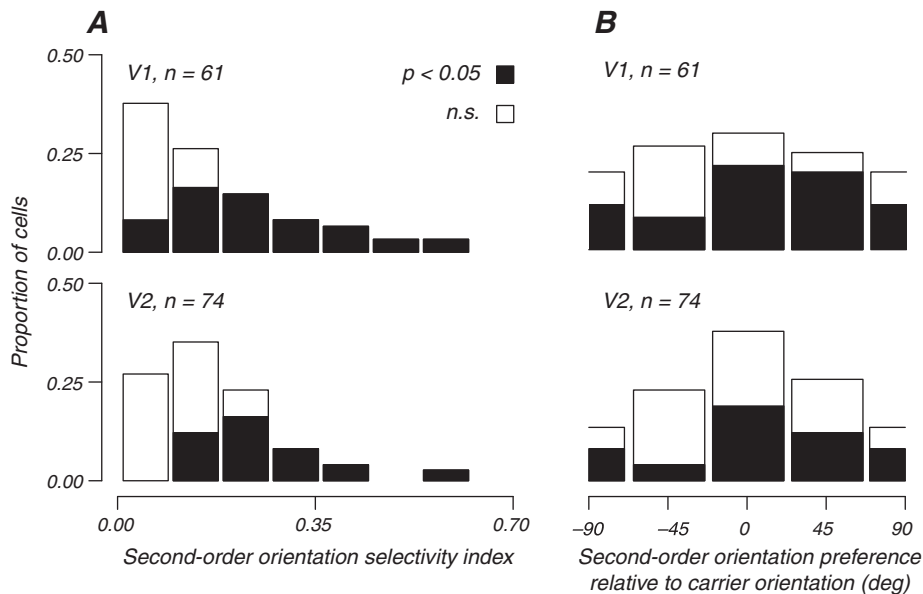


Fig. 3. Second-order orientation selectivity. (A) Distribution of second-order orientation selectivity index (OSI) computed at the moderate modulator spatial frequency ($0.5\times$ carrier grating's spatial frequency). Using a permutation test, we identified neurons with significant second-order OSI ($p < 0.05$, black). For V1, the mean and standard deviation of the OSI were 0.18 and 0.14, respectively. For V2, the mean and standard deviation were 0.17 and 0.12, respectively. (B) Distribution of relative preferred second-order orientation (in deg relative to the carrier grating's orientation) of the four second-order orientations tested. Across the population of neurons, all second-order orientations were represented.

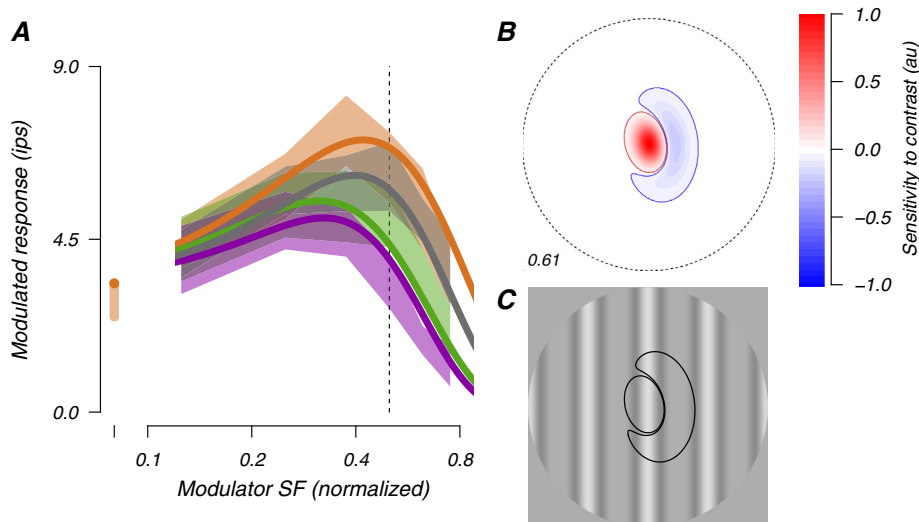


Fig. 4. Model of the spatial organization of the excitatory classical receptive field (CRF) and suppressive extraclassical surround. (A) For neuron *m628r24(V1)*, we computed the response to each modulator spatial frequency and drift direction, and pooled responses to identically oriented modulators that drifted in opposite directions (for this neuron, one spatial frequency and eight directions are shown in Fig. 2B). Different colors pertain to different modulator orientations (0, 45, 90, 135 deg relative to the carrier grating's orientation: orange, gray, purple, green). Shaded regions show standard error of the mean response amplitude across trials. The solid lines show the fitted difference-of-two-spatial-Gaussians model in the frequency domain. These curves capture the organization of the CRF and extraclassical surround. The magnitude of surround suppression is given by the relative response at the optimal modulator spatial frequency (here, approximately $0.4\times$ the carrier grating's spatial frequency) and zero. The vertical, dashed line indicates the modulator spatial frequency (0.79 c/deg) pertaining to the plot in Fig. 2B. At that modulator spatial frequency, the neuron was second-order orientation selective (orientation selectivity index, OSI = 0.15). (B) We inverse Fourier transformed the model fit shown in (A), revealing the spatial organization of the CRF (red) and the extraclassical surround (blue). This center-surround RF describes an envelope of sensitivity to contrast modulations of the carrier grating, and should not be mistaken for a classical simple cell's luminance-responsive receptive field profile. The dashed circle, here and in all other figures, indicates the extent of the stimulus, which comprised eight cycles of the carrier grating. The asymmetric arrangement of the field imparts response selectivity for the orientation of the modulator. To aid visualization, the number at the bottom left (0.61) indicates the overall strength of suppression: the spatially integrated surround divided by the spatially integrated CRF. (C) We superimpose the contours shown in (B) on one of the second-order stimuli (Fig. 1) used to stimulate this neuron. This stimulus cyclically evoked a strong spiking response from the neuron (Fig. 2B) because, periodically, the carrier grating engaged the CRF but was completely withdrawn from the most contrast-sensitive region of the suppressive surround, as shown.

In Fig. 5, we show 25 modeled center-surround RFs. The neurons were diverse in their first-order preferences for the drift direction of a small, circular patch of carrier grating presented to the CRF. In Fig. 5, as in Fig. 4, we have rotated the RFs so that each neuron's

preferred grating is represented as vertical and drifting right. In Fig. 5 the graphical conventions are as in Fig. 4: red and blue indicate the CRF and the extraclassical, suppressive surround, respectively, both of which are sensitive to stimulation by the preferred

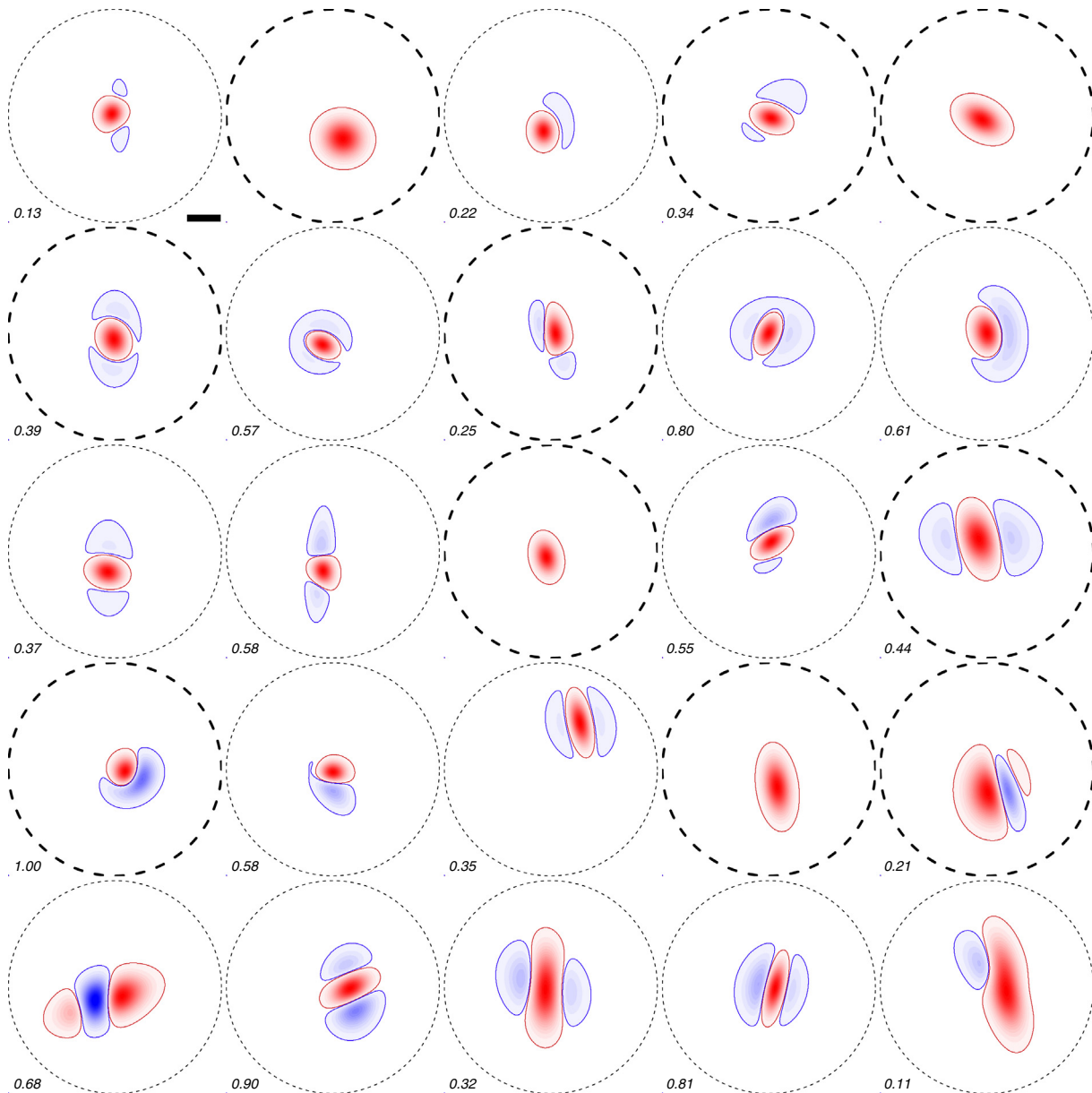


Fig. 5. Modeled spatial organization of the excitatory classical receptive field (red) and suppressive extraclassical surround (blue) of 25 neurons. Graphical conventions are as in Fig. 4B, including the inset number indicating the strength of the suppressive surround if detected. We rotated these receptive fields (RFs), neuron by neuron, so that the (preferred) carrier grating is shown as vertical and drifting to the right. For each RF, the dashed circle indicates the extent of the stimulus, which comprised eight cycles of the carrier grating. The lightly and heavily dashed circles indicate neurons encountered in V1 and V2, respectively. Here, we have ordered RFs left-to-right, top-to-bottom, by second-order orientation selectivity index (OSI) computed at the moderate modulator spatial frequency ($0.5 \times$ carrier grating's spatial frequency). All RFs in the top row have $OSI < 0.10$. RFs in the bottom row have $OSI > 0.4$. The coefficient of validation for all RFs shown was > 0.75 .

grating. For comparison, the field illustrated in Fig. 4 is reproduced in Fig. 5 (row 3, column 1).

Surround suppression is a misnomer; neurons receiving more or less suppression from extraclassical RF subregions at different azimuths to the CRF center are commonly encountered in cat and monkey primary visual cortex (Cavanaugh, Bair, & Movshon, 2002a, 2002b; Tanaka & Ohzawa, 2009; Walker, Ohzawa, & Freeman, 1999). Furthermore, some neurons receive no extraclassical suppression (Walker, Ohzawa, & Freeman, 2000). We saw these patterns in our data. For example, the modeled field of neuron *m617r50(V2)* (Fig. 5, row 4, column 4) showed an elongated CRF (red) but no suppressive surround subregions. This organization agrees with the measured responses to sinusoidal contrast modulations of the preferred carrier grating, which, first, showed no surround suppression when the neuron's field was stimulated

with a large, circular patch of preferred grating, and, second, showed second-order orientation-selectivity at moderate modulator spatial frequencies with modulator (i.e., second-order) orientations parallel to the preferred carrier grating (i.e., 0 deg). The second-order OSI for *m617r50(V2)* was 0.32, which passed a permutation test of selectivity ($p < 0.05$). This neuron was like several others in that modeling revealed no suppressive surround; a 6-parameter model (Section 2), involving a single spatial Gaussian, can adequately modeled the sensitivity of the RF to modulations of the preferred carrier grating.

A second example is illustrated by the model RF of neuron *m616r17(V1)* (Fig. 5, row 4, column 2). That CRF was approximately circular; the suppressive surround was anisotropically organized, being most sensitive immediately below the CRF. This organization agrees with the measured responses to sinusoidal contrast

modulations, which, first, showed marked surround suppression when the neuron's field was stimulated with a large, circular patch of preferred grating. Second, this neuron's responses were second-order orientation-selective at moderate modulator spatial frequencies with modulator orientations perpendicular to the preferred carrier grating (i.e., 90 deg). The second-order OSI for *m616r17(V1)* was 0.27, which passed a permutation test of selectivity ($p < 0.05$).

3.4. Model validation

Model center-surround RFs, like neuron *m616r17(V1)*'s RF (Fig. 5, row 4, column 2), should ideally predict neuronal responses to modulators taking other, non-sinusoidal forms. We validated the model RF of *m616r17(V1)* by measuring neuronal responses to circular patches of preferred carrier grating (Section 2). These patches were diameter $0\times$, $0.17\times$, $0.33\times$, ... $1.0\times$ the diameter of the stimulus shown in Fig. 1, and their overall contrast was modulated between 0 and 0.75 at 0.75 Hz. We compared the measured response to the model's response (scaled to best match in amplitude). As shown in Fig. 6A, for neuron *m616r17(V1)* the coefficient of validation was $R^2 = 0.90$. A second example of validation, this time for neuron *m616r30(V1)*, is shown in Fig. 6B. This neuron's responses showed relatively low second-order orientation-selectivity (OSI = 0.08), consistent with the center-surround RF's organization being more isotropic (cf. *m616r17(V1)*). The extraclassical surround was suppressive, but relatively weak.

For neuron *m637r42(V1)*, we estimated the center-surround RF using spike-triggered averaging. We stimulated the neuron using a stochastic stimulus, as shown in Fig. 7. The preferred carrier grating drifted and the modulator was static, but its spatial frequency and orientation were randomized at 6 Hz. For each spike fired by the neuron we incorporated a modulator into the RF estimate, using the delay that maximized power in the spike-triggered modulator average. The agreement between the spike-triggered RF estimate and the model estimate was acceptable, yielding a similar estimate of the excitatory CRF size, shape and position, and revealing that the extraclassical surround was most suppressive on the CRF's right flank.

3.5. Psychophysics

Could single neurons in human visual cortex with response properties like those described above – especially 2nd-order orientation-selectivity – support human observers' 2nd-order form sensitivity? If so, observers' 2nd-order detection thresholds should show 2nd-order orientation-selectivity. This linking hypothesis is not new – it was recently proposed by Tanaka and Ohzawa (2009), for instance. Nor is the use of 2nd-order adapter stimuli – the method we employed – a novelty; numerous studies have used adaptation to advance a model of 2nd-order SF- and orientation-selective channels (reviewed by Landy & Graham, 2004). But to the best of our knowledge, no psychophysical study has used stimuli like ours (Fig. 1) – 4° stimulus patches presented parafoveally and monocularly – and thus attempted a more direct comparison with single-unit activity.

Further, we hypothesized that cue-invariance would be difficult to evidence psychophysically. In other words, a 1st-order adapter, matched in SF and orientation to a 2nd-order target, should have small effects on 2nd-order sensitivity. This difficulty follows from the fact that primate V1 and V2 neurons are, typically, 1st-order SF- and orientation-tuned, and so an adapter stimulus at a low SF relative to the carrier, or at a relatively oblique angle, is likely to have little effect on the population of neurons encoding 2nd-order form.

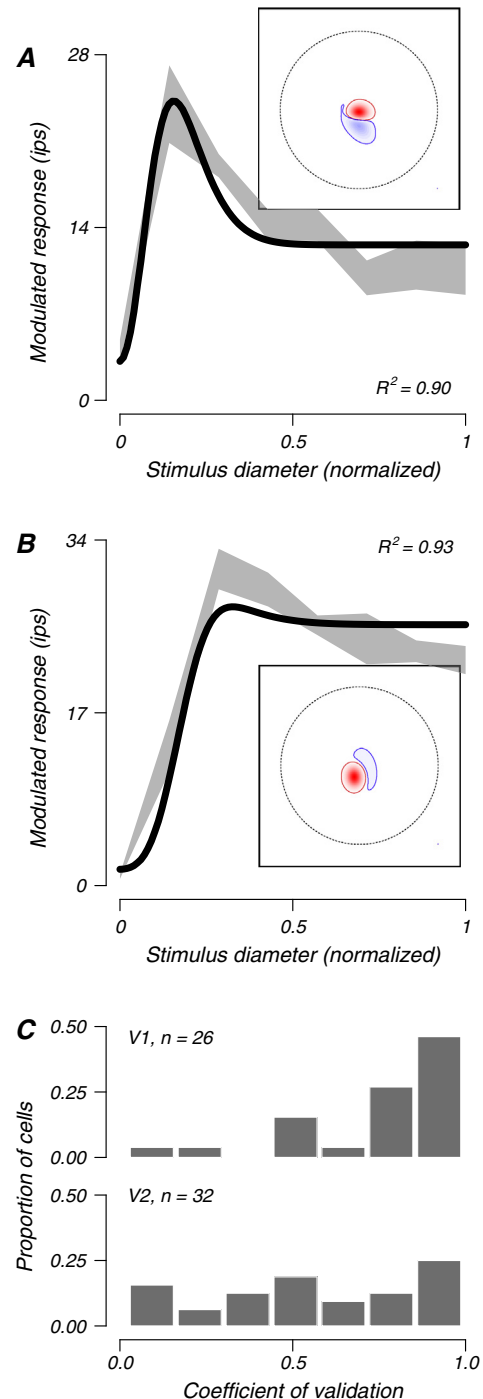


Fig. 6. Validation of the modeled center-surround receptive fields (RFs). (A) For neuron *m616r17(V1)*, we used responses to sinusoidal contrast modulations of the carrier grating (Fig. 1) to model the RF, shown inset using the graphical conventions of Fig. 4B. Then, we stimulated this model RF using circular patches of carrier grating and scaled its response (solid line). The shaded area shows the measured response amplitudes to circular patches (standard error of the mean across trials) which we compared to the modeled response. For this neuron, the coefficient of validation was $R^2 = 0.90$. (B) In neuron *m616r30(V1)*, modeling revealed a weak suppressive surround. The coefficient of validation was $R^2 = 0.93$. Graphical conventions are as in A. (C) Distributions of the coefficient of validation for V1 (upper panel) and V2 (lower panel) neurons that were sufficiently responsive and amenable to modeling over the range of modulator spatial frequencies tested. As in (A and B), we validated the modeled RFs using responses, scaled and offset as necessary, to circular patches of carrier grating.

Psychophysical adaptation affected second-order detection thresholds in a manner consistent with a psychophysical filter-tidy-filter model (reviewed by Landy & Graham, 2004). That

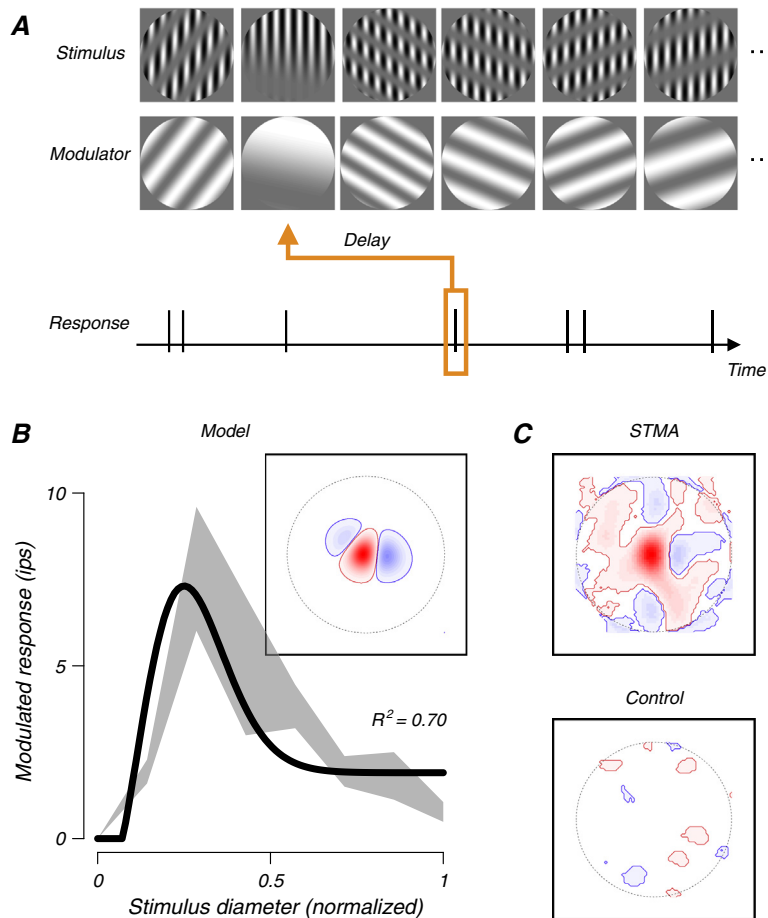


Fig. 7. Center-surround receptive field (RF) estimation using spike-triggered modulator averaging (STMA). (A) We constructed a stochastic stimulus (first row) by multiplying a carrier grating and a modulator (e.g., Fig. 1). In the second row we show the modulator alone. The carrier grating drifted and the modulator was static but its spatial frequency and orientation were randomized at 6 Hz; spatial frequency was drawn from a uniform distribution on $[0, 0.75]$ cycles/deg relative to the carrier, and orientation was drawn from a uniform distribution on $[0, 180]$ degrees. For each spike, we incorporated a modulator into the average using the delay (orange arrow) that maximized STMA power. (B) For neuron *m637r42(V1)*, we used responses to sinusoidal contrast modulations of the 4 c/deg carrier grating to model the RF. The model revealed how neuron achieved second-order orientation selectivity, responding vigorously to vertical but not horizontal contrast modulations: via strong surround suppression (blue) on the right flank of the excitatory classical receptive field (CRF) shown in red. Graphical conventions are as in Fig. 6. (C) We estimated *m637r42(V1)*'s center-surround RF using STMA (upper panel). Note the agreement with the model RF in (B): in the STMA, the surround was most suppressive on the right flank of the CRF. We used an implausible delay (-100 ms) to generate a control STMA (lower panel) which showed no RF structure.

model proposes that observer sensitivity is subserved by channels, each involving two cascaded stages. The first stage produces a rectified, orientation and spatial frequency selective response to the sinusoidal carrier grating (Langley, Fleet, & Hibbard, 1996). The second stage, which is bandpass and tuned to a relatively low spatial frequency (Ellemberg, Allen, & Hess, 2006; Landy & Oruç, 2002), responds in an orientation-selective way to contrast modulations. However, adaptation affected thresholds in a manner largely inconsistent with a psychophysical model that is cue-invariant. A cue-invariant model involves channels responding indiscriminately to (first-order) luminance modulations and (second-order) contrast modulations with the same orientation and spatial frequency. But as shown in Fig. 8, thresholds for the detection of a second-order contrast modulation remained low when the adapter was a luminance grating, and were affected little by the luminance adapter's orientation. The notion of a cue-invariant psychophysical model follows from single-unit recordings in cat area 18 showing indiscriminate responses to luminance and contrast modulations of the same spatial frequency and orientation (Li & Baker, 2012). But there is little psychophysical evidence for channels that are invariant across the cues of both luminance and contrast (as evidenced by this psychophysical result, and others).

4. Discussion

We stimulated single units in V1 and V2 with stimuli composed of a preferred carrier grating – which vigorously activated the neuron during hand mapping – whose contrast we modulated with drifting raised sinusoids. We modeled RF organization using the difference of spatial Gaussians that were sensitive to contrast (not luminance) changes of the carrier grating. This model is an instantiation of a psychophysical model (Landy & Graham, 2004) which can account for the sensitivity of human observers to second-order features defined by contrast, orientation, or spatial frequency; we were interested in this model's ability to account for the responses of single neurons, potentially linking this neuronal response phenomenon to perception. Our main findings are summarized as follows. Many neurons responded selectively to the orientation of the contrast modulation of the preferred carrier grating, that is, the majority of neurons were second-order orientation selective. Modeling revealed diverse organizations of classical receptive field (CRF) and extraclassical, suppressive surround, and suggested that second-order selectivity arises from both elongated excitatory CRFs, asymmetrically organized surround suppression, or both.

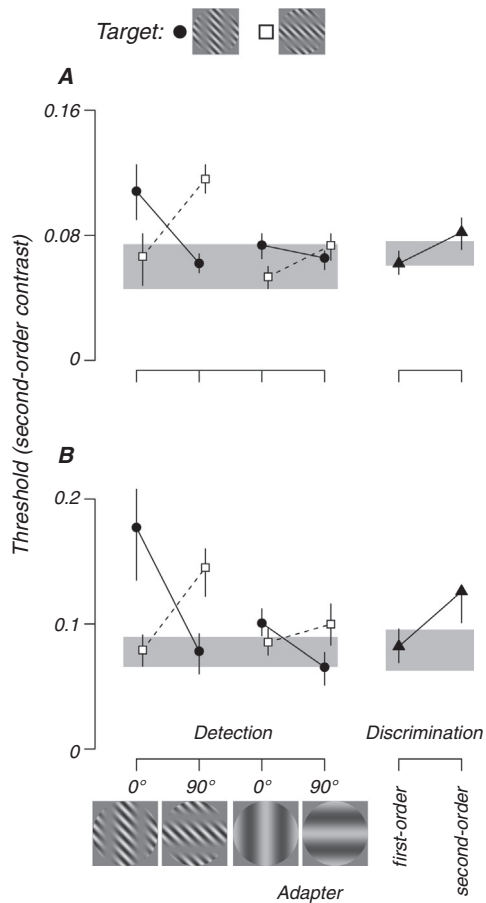


Fig. 8. Second-order psychophysical detection and discrimination. Two observers' second-order thresholds were affected by adaptation in a way that was consistent with a filter-rectify-filter model that is selective for second-order orientation. (A) Subject 1's threshold for the detection of a 0.5 c/deg, vertical contrast modulation of an oblique, 2 c/deg grating (circles) was elevated by a vertical, second-order adapter, but not by a horizontal, second-order adapter. Nor was this threshold elevated by 0.5 c/deg vertical or horizontal luminance gratings. Thresholds for the detection of a horizontal contrast modulation (squares) showed the corresponding pattern. The gray bands show the 95% confidence interval of the detection threshold for a horizontal, second-order target when the adapter was a uniform, mean-luminance field. The right panel shows that discrimination thresholds (second-order vertical vs. second-order horizontal) were increased by second-order adapters, but remained relatively low for 1st-order adapters. The gray band again shows the 95% confidence interval of the discrimination threshold when the adapter was a uniform, mean-luminance field. (B) Thresholds for subject 2. Graphical conventions are as in (A). Error bars show 95% confidence intervals.

We modeled the CRF and the extraclassical surround by assuming two spatially distinct mechanisms, one excitatory and the other suppressive. We converted the span of receptive fields from degrees of visual angle to millimeters in cortex to give insight into the governing neural circuit. Our measurements may improve on previous work (e.g., Cavanaugh, Bair, and Movshon (2002a), Sceniak et al. (1999)), because using sinusoidally modulated carrier gratings, as opposed to circular and annular grating patches, may immunize our results to biases arising from anisotropic center-surround organization and/or imprecise stimulus centering. Our model revealed the excitatory mechanism's maximum radius (2σ) to be 0.58 deg on average, that is, 1.74 mm in cortex assuming a cortical magnification factor of 3 mm/deg for our parafoveal recordings (Gattass, Gross, & Sandell, 1981; Tootell et al., 1988; Van Essen, Newsome, & Maunsell, 1984) (Fig. 9). In agreement with Cavanaugh, Bair, and Movshon (2002a), this radius spans several cortical columns and is comparable to the extent of horizontal intracortical connections mediated by recurrent collaterals of

pyramidal cell axons (Angelucci et al., 2002; Braitenberg & Schüz, 1991). When our model revealed suppression, it was stronger nearer the CRF, consistent with previous studies of neuronal responses in V1 using circular and/or annular patches of grating (Bair, Cavanaugh, & Movshon, 2003; Cavanaugh, Bair, & Movshon, 2002a, 2002b; Sceniak et al., 1999; Shushruth et al., 2013). But we found little evidence in either our model fits or in responses to grating patches of suppression from regions remote from the CRF.

Our model fits seem mostly to reflect the "near" component of suppression proposed by Angelucci, Levitt, and Lund (2002) and Angelucci et al. (2002). That mechanism is proposed to be relatively strong, and narrowly orientation-tuned, and perhaps dependent on local long-range horizontal connections as well as cortico-cortical feedback (Gilbert & Wiesel, 1989; Yoshioka et al., 1996). On average, the suppressive extraclassical surround was $1.65\times$ wider than the excitatory mechanism largely responsible for the CRF (Fig. 9), smaller than the full surround reported in a number of previous studies (Angelucci, Levitt, & Lund, 2002; Angelucci et al., 2002; Cavanaugh, Bair, & Movshon, 2002a, 2002b; Levitt & Lund, 1997; Sceniak et al., 1999), some of which found suppression more than 6 deg from the CRF. Why the discrepancy? One possible explanation is adaptation: we stimulated without interleaved, mean-luminance blank stimuli, and the extraclassical suppressive surround is more susceptible to contrast adaptation than the CRF (Cavanaugh, Bair, & Movshon, 2002a). Another possible explanation is stimulus contrast: on average, we used moderate contrast (0.38), which weakens the suppressive effects of the extraclassical surround (Cavanaugh, Bair, & Movshon, 2002a; Sceniak et al., 1999), whereas previous studies of primate V1 have tended to use higher contrast. In additional, preliminary experiments, we lowered the contrast of the preferred carrier grating (Fig. 1), and summed the resulting stimulus with a second, orthogonal carrier grating (unpublished observations). We found little effect of that orthogonal carrier beyond the CRF, suggesting that the surround mechanism captured by our modeling is strongly orientation-tuned, like the "near" surround of Angelucci and colleagues.

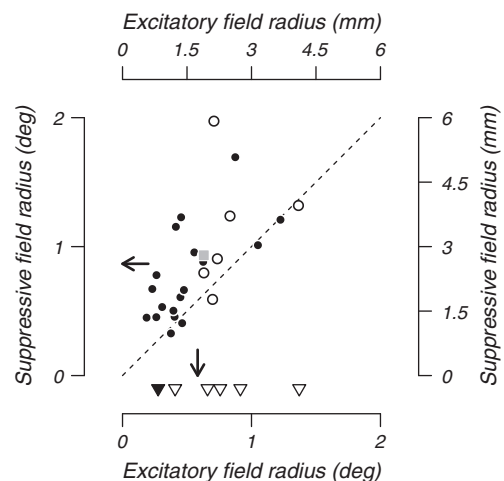


Fig. 9. Scatter plot of the maximum radius (2σ) of model excitatory classical receptive field (CRF) and suppressive extraclassical surround, showing the 20 V1 neurons (●, ▼) and 11 V2 neurons (○, ▽) that survived both modeling and validation (validation score > 0.75). The model revealed surround suppression in 25 neurons (circles) and excitation only (i.e., no suppression) in six others (triangles). To convert visual angle (deg) to cortical radius (mm), we assumed a cortical magnification factor of 3 mm/deg, appropriate to our parafoveal eccentricities. Arrows show excitatory and suppressive means, and the gray square indicates a cortical magnification factor of 3 mm/deg, appropriate to our parafoveal eccentricities. On average, the suppressive extraclassical surround was $1.65\times$ wider than the excitatory mechanism largely responsible for the CRF.

Our analysis assumes that excitatory and suppressive mechanisms are spatially distinct, but responded with identical time courses. The latter assumption is not strictly correct: suppressive signals tend to be delayed by 10–20 ms from the center excitation (Bair, Cavanaugh, & Movshon, 2003; Hupé et al., 2001; Xing et al., 2005; but see Webb et al., 2005). But our low modulator drift rate (0.75 Hz) renders the small delay of suppression inconsequential. Not unexpectedly, there was therefore little evidence in neurons' responses to stimuli that separate estimates of RF center and surround latencies would have improved the fit.

The single-unit second-order selectivity that Tanaka and Ohzawa (2009) described in the cat and that we confirm here in the primate, is fundamentally different from the second-order selectivity described by Baker and colleagues (Li & Baker, 2012; Mareschal & Baker, 1998; Zhou & Baker, 1994). There, single units in cat visual cortex responded to small stimuli presented to the CRF. Those stimuli comprised a sinusoidal contrast modulation of a very high spatial frequency sinusoidal carrier grating, well beyond the passband of spatial frequencies which, in the absence of a contrast modulation, elicited neuronal responses. Those responses were second-order-selective and also cue-invariant, showing similar orientation and spatial frequency preferences for an ordinary luminance grating and modulator imposed on a very high spatial frequency carrier grating alike. Our stimuli, on the other hand, were large, circular patches comprising sinusoidal contrast modulations of a preferred carrier grating which, when used to stimulate the CRF in the absence of any contrast modulation, elicited vigorous responses. Our psychophysical data showed that a first-order adapter has relatively small effects on second-order detection and discrimination thresholds. This result, and the psychophysical results of many others (e.g., Dakin & Mareschal, 2000; Langley, Fleet, & Hibbard, 1996; Schofield & Georgeson, 1999), provide evidence for separate first- and second-order psychophysical mechanisms, suggesting that cue invariant neurons, if indeed they can be found in primate early visual cortex, play a minor role in the perception of spatial forms.

It is attractive to consider our neuronal responses in light of human psychophysical responses. There are a number of points of agreement. Langley, Fleet, and Hibbard (1996), using second-order, contrast-modulated targets like our stimulus components (Fig. 1), showed that second-order orientation discrimination depends on two stages of processing. The first stage is tuned to the spatial frequency and orientation of luminance modulations and rectified. The second stage is spatial frequency and orientation tuned to contrast modulations per se. In all, this two-stage processing is like the neuronal responses we measured. First, we isolated neurons with CRFs that were selectively sensitive to the spatial frequency and orientation of a grating. Second, responses were selectively modulated by the appearance of oriented, second-order contrast differences across the center-surround RF.

In summary, we believe that our results provide the long-sought psychophysical substrate for second-order contrast perception. Instead of being represented by a wholly separate class of responses or neurons (cf. El-Shamayleh & Movshon, 2011; Li & Baker, 2012), we find that the long-studied suppressive surround of cortical cells allows them to do double duty as detectors of both first- and second-order contrast. Just as Wiesel and Hubel's (1966) "type 3" cells in the LGN do double duty as detectors of color and form, cortical cells in V1 and V2 carry two distinct kinds of form signal, which could – like color and form – be decoded and if necessary separately processed by downstream areas.

Acknowledgments

Thanks to Norma Graham for comments on an early draft of the manuscript. Romesh Kumbhani, Christopher Shooner, Brett Vintch,

Corey Ziemba, Robbe Goris and Yasmine El-Shamayleh participated in experiments and were generally invaluable. This study was supported by the Australian National Health & Medical Research Council fellowship 1016388 to L.H. and the U.S. National Institutes of Health Grant NIH EY 04440 to J.A.M.

References

- Angelucci, A., Levitt, J. B., Walton, E. J., Hupe, J. M., Bullier, J., & Lund, J. S. (2002a). Circuits for local and global signal integration in primary visual cortex. *Journal of Neuroscience*, 22(19), 8633–8646.
- Angelucci, A., Levitt, J. B., & Lund, J. S. (2002b). Anatomical origins of the classical receptive field and modulatory surround field of single neurons in macaque visual cortical area V1. *Progress in Brain Research*, 136, 373–388.
- Bair, W., Cavanaugh, J. R., & Movshon, J. A. (2003). Time course and time–distance relationships for surround suppression in macaque V1 neurons. *Journal of Neuroscience*, 23(20), 7690–7701.
- Braitenberg, V., & Schüz, A. (1991). *Anatomy of the cortex: Statistics and geometry*. Berlin: Springer-Verlag.
- Carandini, M., & Heeger, D. J. (2013). Normalization as a canonical neural computation. *Nature Reviews Neuroscience*, 14(2), 51–62.
- Cavanaugh, J. R., Bair, W., & Movshon, J. A. (2002a). Nature and interaction of signals from the receptive field center and surround in macaque V1 neurons. *Journal of Neurophysiology*, 88(5), 2530–2546.
- Cavanaugh, J. R., Bair, W., & Movshon, J. A. (2002b). Selectivity and spatial distribution of signals from the receptive field surround in macaque V1 neurons. *Journal of Neurophysiology*, 88(5), 2547–2556.
- Dakin, S. C., & Mareschal, I. (2000). Sensitivity to contrast modulation depends on carrier spatial frequency and orientation. *Vision Research*, 40(3), 311–329.
- De Valois, R. L., William Yund, E., & Hepler, N. (1982). The orientation and direction selectivity of cells in macaque visual cortex. *Vision Research*, 22(5), 531–544.
- Ellemberg, D., Allen, H. A., & Hess, R. F. (2006). Second-order spatial frequency and orientation channels in human vision. *Vision Research*, 46(17), 2798–2803.
- El-Shamayleh, Y., & Movshon, J. A. (2011). Neuronal responses to texture-defined form in macaque visual area V2. *Journal of Neuroscience*, 31(23), 8543–8555.
- Enroth-Cugell, C., & Robson, J. G. (1966). The contrast sensitivity of retinal ganglion cells of the cat. *Journal of Physiology*, 187(3), 517–552.
- Gattass, R., Gross, C. G., & Sandell, J. H. (1981). Visual topography of V2 in the macaque. *Journal of Comparative Neurology*, 201(4), 519–539.
- Gilbert, C. D., & Wiesel, T. N. (1989). Columnar specificity of intrinsic horizontal and corticocortical connections in cat visual cortex. *Journal of Neuroscience*, 9(7), 2432–2442.
- Graham, N. V. (2011). Beyond multiple pattern analyzers modeled as linear filters (as classical V1 simple cells): Useful additions of the last 25 years. *Vision Research*, 51(13), 1397–1430.
- Graham, N., & Sutter, A. (1998). Spatial summation in simple (Fourier) and complex (non-Fourier) texture channels. *Vision Research*, 38(2), 231–257.
- Graham, N., & Wolfson, S. S. (2004). Is there opponent-orientation coding in the second-order channels of pattern vision? *Vision Research*, 44(27), 3145–3175.
- Green, D. M., & Swets, J. A. (1966). *Signal detection theory and psychophysics*. New York: Wiley.
- Henry, C. A., Joshi, S., Xing, D., Shapley, R. M., & Hawken, M. J. (2013). Functional characterization of the extraclassical receptive field in macaque V1: Contrast, orientation, and temporal dynamics. *Journal of Neuroscience*, 33(14), 6230–6242.
- Hupé, J. M., James, A. C., Girard, P., & Bullier, J. (2001). Response modulations by static texture surround in area V1 of the macaque monkey do not depend on feedback connections from V2. *Journal of Neurophysiology*, 85(1), 146–163.
- Kim, T., & Freeman, R. D. (2014). Selective stimulation of neurons in visual cortex enables segregation of slow and fast connections. *Neuroscience*, 274, 170–186.
- Landy, M. S., & Graham, N. V. S. (2004). In L. M. Chalupa & J. S. Werner (Eds.), *The visual neurosciences* (pp. 1106–1118). Cambridge MA: MIT Press.
- Landy, M. S., & Bergen, J. R. (1991). Texture segregation and orientation gradient. *Vision Research*, 31(4), 679–691.
- Landy, M. S., & Oruç, I. P. (2002). Properties of second-order spatial frequency channels. *Vision Research*, 42(19), 2311–2329.
- Langley, K., Fleet, D. J., & Hibbard, P. B. (1996). Linear filtering precedes nonlinear processing in early vision. *Current Biology*, 6(7), 891–896.
- Levitt, J. B., Kiper, D. C., & Movshon, J. A. (1994). Receptive fields and functional architecture of macaque V2. *Journal of Neurophysiology*, 71(6), 2517–2542.
- Levitt, J. B., & Lund, J. S. (1997). Contrast dependence of contextual effects in primate visual cortex. *Nature*, 387(6628), 73–76.
- Li, G., & Baker, C. L. Jr., (2012). Functional organization of envelope-responsive neurons in early visual cortex: Organization of carrier tuning properties. *Journal of Neuroscience*, 32(22), 7538–7549.
- Mareschal, I., & Baker, C. L. Jr., (1998). A cortical locus for the processing of contrast-defined contours. *Nature Neuroscience*, 1(2), 150–154.
- McGraw, P. V., Levi, D. M., & Whitaker, D. (1999). Spatial characteristics of the second-order visual pathway revealed by positional adaptation. *Nature Neuroscience*, 2(5), 479–484.
- Ringach, D. L., Hawken, M. J., & Shapley, R. (1997). Dynamics of orientation tuning in macaque primary visual cortex. *Nature*, 387(6630), 281–284.
- Rodieck, R. W., & Stone, J. (1965). Analysis of receptive fields of cat retinal ganglion cells. *Journal of Neurophysiology*, 28(5), 833–849.

- Ross, J., & Speed, H. D. (1991). Contrast adaptation and contrast masking in human vision. *Proceedings of the Royal Society of London. Series B: Biological Sciences*, 246(1315), 61–70.
- Saarela, T. P., & Landy, M. S. (2012). Combination of texture and color cues in visual segmentation. *Vision Research*, 58, 59–67.
- Sceniak, M. P., Ringach, D. L., Hawken, M. J., & Shapley, R. (1999). Contrast's effect on spatial summation by macaque V1 neurons. *Nature Neuroscience*, 2, 733–739.
- Schofield, A. J., & Georgeson, M. A. (1999). Sensitivity to modulations of luminance and contrast in visual white noise: Separate mechanisms with similar behaviour. *Vision Research*, 39(16), 2697–2716.
- Shushruth, S., Nurminen, L., Bijanzadeh, M., Ichida, J. M., Vanni, S., & Angelucci, A. (2013). Different orientation tuning of near-and far-surround suppression in macaque primary visual cortex mirrors their tuning in human perception. *Journal of Neuroscience*, 33(1), 106–119.
- Tanaka, H., & Ohzawa, I. (2009). Surround suppression of V1 neurons mediates orientation-based representation of high-order visual features. *Journal of Neurophysiology*, 101(3), 1444–1462.
- Tanner, W. P., Jr., & Swets, J. A. (1954). A decision-making theory of visual detection. *Psychological Review*, 61(6), 401.
- Tootell, R. B., Switkes, E., Silverman, M. S., & Hamilton, S. L. (1988). Functional anatomy of macaque striate cortex. II. Retinotopic organization. *Journal of Neuroscience*, 8(5), 1531–1568.
- Van Essen, D. C., Newsome, W. T., & Maunsell, J. H. (1984). The visual field representation in striate cortex of the macaque monkey: Asymmetries, anisotropies, and individual variability. *Vision Research*, 24(5), 429–448.
- Walker, G. A., Ohzawa, I., & Freeman, R. D. (1999). Asymmetric suppression outside the classical receptive field of the visual cortex. *Journal of Neuroscience*, 19(23), 10536–10553.
- Walker, G. A., Ohzawa, I., & Freeman, R. D. (2000). Suppression outside the classical cortical receptive field. *Visual Neuroscience*, 17(03), 369–379.
- Watson, A. B., & Robson, J. G. (1981). Discrimination at threshold: Labeled detectors in human vision. *Vision Research*, 21(7), 1115–1122.
- Webb, B. S., Dhruv, N. T., Solomon, S. G., Tailby, C., & Lennie, P. (2005). Early and late mechanisms of surround suppression in striate cortex of macaque. *Journal of Neuroscience*, 25(50), 11666–11675.
- Wichmann, F. A., & Hill, N. J. (2001a). The psychometric function: I. Fitting, sampling, and goodness of fit. *Perception & Psychophysics*, 63(8), 1293–1313.
- Wichmann, F. A., & Hill, N. J. (2001b). The psychometric function: II. Bootstrap-based confidence intervals and sampling. *Perception & Psychophysics*, 63(8), 1314–1329.
- Wiesel, T. N., & Hubel, D. H. (1966). Spatial and chromatic interactions in the lateral geniculate body of the rhesus monkey. *Journal of Neurophysiology*, 29(6), 1115–1156.
- Xing, D., Shapley, R. M., Hawken, M. J., & Ringach, D. L. (2005). Effect of stimulus size on the dynamics of orientation selectivity in macaque V1. *Journal of Neurophysiology*, 94(1), 799–812.
- Yoshioka, T., Blasdel, G. G., Levitt, J. B., & Lund, J. S. (1996). Relation between patterns of intrinsic lateral connectivity, ocular dominance, and cytochrome oxidase-reactive regions in macaque monkey striate cortex. *Cerebral Cortex*, 6(2), 297–310.
- Zhou, Y. X., & Baker, C. L. (1994). Envelope-responsive neurons in areas 17 and 18 of cat. *Journal of Neurophysiology*, 72(5), 2134–2150.